encit 2020

ABCM Associação Brasileira de Engenharia e Ciências Mecânicas

18th Brazilian Congress of Thermal Sciences and Engineering
November 16-20, 2020 (Online)

ENC-2020-0506
INVESTIGATION OF DIRECT ETHANOL INJECTION PRESSURE AND TIMING PARAMETERS ON COMBUSTION, PERFORMANCE AND EMISSION IN PART LOAD OF A SPARK IGNITION ENGINE

Diego Golke
Universidade Federal do Rio Grande do Sul
Av. Paulo Gama, 110, Bairro Farroupilha, Porto Alegre, Rio Grande do Sul
CEP: 90040-060, Fone: 55 (51) 33086000
diego.golke@gmail.com

Mario Eduardo Santos Martins
Thompson Diórdinis Metzka Lanzanova
Geovane Alberto Frizzo Prante
Marcelo Rohrig
Roberto Antonio Garlet
Universidade Federal de Santa Maria
Av. Roraima, nº 1000, Cidade Universitária, Bairro Camobi, Santa Maria - RS
CEP: 97105-900 ,55 (55) 3220-7906
mario@mecnica.ufsm.br

Abstract. *Over the past decades, internal combustion engines (ICEs) have struggled with ever stringent emission legislation. Nowadays, the downsizing concept is becoming largely employed in spark ignition engines due to increased engine efficiency. However, the presence of turbocharging and direct fuel injection system makes the strategies of engine management for drivability more complex and needs further investigation with the specifics of the Brazilian market, in which hydrous ethanol is widely available. Hence, this work intends to study the effects on emissions and combustion performance parameters by varying direct injection timing and pressure at part load of a three-cylinder 1.0 L turbocharged engine. The engine was fueled with hydrous ethanol, which is expected have increased usage in Brazil. The tests were carried out at 2 and 8 bar IMEP, 1500 rpm and stoichiometric condition. The spark timing was adjusted to maintain CA50 in 10 CAD ATDCf and the positive valve overlap was of 20 CAD symmetrical at TDC. The injection pressure and injection timing were swept from 60 to 140 bar and 0 to 120 CAD ATDCi respectively. The results showed in part load an optimum injection timing at 30 CAD ATDCi. The injection pressure effect showed more influence in late injection, improving engine stability and emissions.*

Keywords: *Ethanol, injection timing, injection pressure, part load, direct injection.*

1. INTRODUCTION

Several efforts have been made to increase energy efficiency and it is still necessary to progressively slow down the growth in energy demand (ExxonMobil 2019). In Brazil, the new phase of the vehicle emission control program (PROCONVE – L7) will start in 2022 (MMA 2018). The objective is decrease carbon dioxide (CO_2) emitted per km while improving urban air quality by reducing pollutants. Some author worldwide, as example (Economist 2017), are proposing the end of internal combustion engines (ICEs) production to be replaced by electric motors to further reduce emissions. In this scenario, battery electric vehicles (BEVs) looks a suitable alternative to ICEs. However, a life cycle assessment shows some problems that need be overcome by BEVs to become a reliable and widespread technology. For instance, 49% of the CO_2 emitted comes from electricity generation and heating against 20% from the transport sector (Hannah Ritchie and Max Roser 2020). Thus, the electricity that feed BEVs needs be produced from carbon free energy. Otherwise, the growth use of BEVs could further increases the greenhouse gas (GHG) emissions. However, a simplified calculation carried out by (Pielke 2019) showed that achieving a net zero CO2 emission by 2050 is a difficult task. In addition, others problems are related with the batteries, for instance: energy density, recharging time, durability and raw material supply (Serrano 2017). Indeed, stop the ICEs production could lead environmental problems as well as economics, social and political problems without the tax on ICEs and fuels mainly in emerging economies (Kalghatgi 2018). The continuous efficiency improvement of ICEs is the only way to overcome the challenging task from strict vehicle emissions legislation (Kalghatgi 2019).

Downsizing engines are already largely employed in developed countries to further improve engine efficiency. Engine efficiency improvement with this concept is due mainly by reduced displacement volume, which reduce the engine friction and decrease pumping losses as engine operate in high load more frequently (Bassett et al. 2017). In addition, fuel direct injection (DI) system is frequently used with downsized turbocharged engine (Hancock et al. 2008). The advantages of DI system is the possibility of engine operating with stratified or homogenous combustion, and the cooling effect that reduces knock probability (Fraser et al. 2009; Chincholkar and Suryawanshi 2016). However, these technologies added to the engine make the management strategies for drivability more complicated and needs further investigation with the specifics of the Brazilian market such as hydrous ethanol.

In Brazil, hydrous ethanol is again a promising alternative to gasoline mainly due to governmental incentive programs such as RenovaBio (Agência Nacional do Petróleo Gás Natural e Biocombustíveis - ANP n.d.). When compared with gasoline, ethanol has higher octane number and therefore greater knock resistance (Diego Golke et al. 2018; Stein, House, and Leone 2009). Also, hydrous ethanol has higher latent heat of vaporization than gasoline (Thewes et al. 2012), which could increase the charge cooling effect. Both characteristics are highly suitable for DI turbocharged engine because they allow higher compression ratio and with reduced WOT fuel enrichment (Leone et al. 2015). However, in part load, the pumping work is increased due the greater density of air resulted from the cooling effect. Thus, intake pressure is lower to maintain same engine load. Yet, the compression work is decreased by the lower temperature and pressure (Nakata et al. 2006). In addition, hydrous ethanol demands less energy for production compared to anhydrous ethanol (Sari et al. 2017) and offers lower cost. Studies carried out by (T. D. M. Lanzanova, Dalla Nora, and Zhao 2016; Sari et al. 2018) showed the hydrous ethanol potential on engine performance and emissions. Other characteristics that can increase the engine efficiency are given by the higher ratio of specific heat than gasoline (Germane, Wood, and Hess 1983), and by the greater amounts of triatomic molecules produced during combustion that increase the mixture heat capacity, decreasing the temperature and reducing the heat losses (Zhang et al. 2015). Also, the combustion duration can decrease as well as the heat losses due the ethanol higher laminar flame speed than gasoline (Yu et al. 2019). Nevertheless, hydrous ethanol has reduced lower heating value (LHV) than gasoline, which increases the fuel consumption and reduces fuel tank mileage (D. Golke et al. 2016).

An investigation of injection timing was carried out by Lanzanova *et al.* (T. Lanzanova et al. 2017) in a single cylinder spark ignition (SI) DI engine using gasoline. The injection pressure was maintained at 145 bar, 6 bar of indicated mean effective pressure (IMEP), engine speed of 1500 rpm and spark ignition adjusted to minimum spark advance for best torque (MBT). The result showed higher cooling effect and decreased emissions of nitrogen oxides (NO_X) as delayed injection timing. However, the combustion efficiency was impaired as retarded injection timing due higher carbon monoxide (CO) and hydrocarbons (HC) emissions.

This paper then presents an investigation of injection timing and pressure effect on performance, combustion and emissions parameters. The tests were carried out in a three cylinders DI turbocharged Ford EcoBoost 1.0 liters engine fueled with hydrous ethanol. The crank angle degree (CAD) of 50% mass fraction burned (CA50) was maintained at 10 CAD after top dead center firing (ATDCf) and the coefficient of variation of IMEP (COV_{IMEP}) was limited at 3%. The engine speed was fixed at 1500 rpm and the engine load were 2 and 8 bar IMEP. A positive valve overlap of 20 CAD was used and stoichiometric air – fuel ratio. The injection timing was swept from 0 to 120 after top dead center from intake stroke (ATDCi) and injection pressure from 60 to 140 bar.

2. METHODOLOGY

2.1 Mathematical equations

The in-cylinder pressure are recorded as function of CAD and the volume matrix is given by

$$V = V_c(1 + \frac{1}{2}(r_c - 1)[R + 1 - \cos CAD - (R^2 - \sin^2 CAD)^{\frac{1}{2}}] \quad (1)$$

Where V_c is the clearance volume, r_c is the compression ratio and R is the ratio of connecting rod length to crank radius. The in-cylinder work by definition is calculated as

$$\delta w = F.dx = P.A.dx = P.dv \quad (2)$$

Where w means specific work, P is the in-cylinder pressure and v is the specific volume. In this way, the Eq. (2) is integrated to account the in-cylinder work. A numerical method, as instance trapezoidal rule, is commonly used to integrate the area from pressure versus volume diagram. Then, the in-cylinder work is obtained as

$$W = \sum_{i=1}^{n} \frac{1}{2}(P_{i-1} + P_i)\Delta V_i \quad (3)$$

The analysis of heat release is performed by applying the first law of thermodynamic in an open system boundary and treating as a single zone model with an average temperature, resulting in a general formulation as

$$\delta Q_{ch} = \delta Q_{ht} + dU_s + \delta W + \sum h_i dm_i \quad (4)$$

Where Q_{ch} is the chemical energy, U_s sensible energy, Q_{ht} heat transfer and $\sum h_i dm_i$ energy transferred through the boundary. The sensible energy can be written as $U_s = mu(T)$, where T stands for average gas temperature in-cylinder. The derivative of sensible energy results in

$$dU_s = dm.u(T) + m.du(T) \quad (5)$$

For ideal gas law, the sensible energy could be estimated by a relation measured in a special process as shown by (Bejan 2016). In such manner, the Eq. (5) is replaced in Eq. (4)

$$\delta Q_{ch} = \delta Q_{ht} + dm.u(T) + m.c_v T + Pdv + \sum h_i dm_i \quad (6)$$

The in-cylinder mass variation (dm_i) is due the mass crevice leaking, thus

$$dm_i = -dm = dm_{cr} \quad (7)$$

The derived form of the ideal gas law is used to swap the term $m.c_v dT$ in Eq. (6)

$$PV = mRT \rightarrow dP.V + PdV = mRdT + dmRT \quad (8)$$

Where R (universal constant) was considered constant. Substituting the Eq. (8) and Eq. (7) in Eq. 6 and using the following relation $cv(\gamma - 1) = R$

$$\delta Q_{ch} - (h' - u + cvT)dm_{cr} - \delta Q_{ht} = Pdv\left(\frac{1}{(\gamma-1)} + 1\right) + \frac{1}{(\gamma-1)} vdP \quad (9)$$

The right side is known as apparent or net heat release, therefore, the final equation as function of CAD is written as

$$\frac{\delta Q_{apparent}}{d\theta} = P\frac{dv}{d\theta}\left(\frac{1}{(\gamma-1)} + 1\right) + \frac{1}{(\gamma-1)} v\frac{dP}{d\theta} \quad (10)$$

The calculation of the mass fraction burned curve was based in the integration of the apparent heat release rate. Therefore, CAD 10, 50 and 90 were determined from the normalized curve carried out after the integrated apparent heat release curse. The engine load was calculated considering the net indicated engine work, thus

$$IMEP = \frac{\oint_{-360}^{+360} p_i dV}{Vd} = \frac{W_{c,i}}{Vd} \quad (11)$$

Where Vd means displaced volume. The indicated efficiency, which means the energy of conversion of the fuel into work for the piston, was calculated by

$$\eta_i = \frac{IMEP\, V_d}{m_{fuel,c}\, LHV_{fuel}} \quad (12)$$

Where $m_{fuel,c}$ is the mass fuel injected and LHV_{fuel} is the lower heat value. The coefficient of variance of the engine was calculated over the IMEP and in 300 cycles. This parameter is related to drivability problems and concerns the cyclical variability of the work delivered per cycle

$$COV_{IMEP}(100\%) = \frac{\sigma_{IMEP}}{IMEP_{average}} * 100 \quad (13)$$

Where σ_{IMEP} is the standard deviation of IMEP. Combustion efficiency concerns fuel energy wasted as a result of incomplete combustion. The combustion efficiency is calculated by

$$\eta_c = 1 - \frac{\sum \dot{m}_i LHV_i}{\dot{m}_{fuel} LHV_{fuel}} \quad (14)$$

Where i indicates exhaust gases such as CO and hydrocarbons. The concentrations of CO, hydrocarbons and NO_X were measured in ppm and in wet basis. However, in order to have more representative results in view of a comparative analysis, the emissions were passed from ppm to g / kW.h according to the standard (Economic Commission for Europe of the United Nations 2013). The conversion of CO, hydrocarbons and NO_x from ppm to g / kW.h took place as follows:

$$ISCO = \frac{\frac{MW_{CO}}{MW_{mix}}[CO]\dot{m}_{exh}}{P_i} \quad (15)$$

$$ISNO_x = \frac{\left(\Sigma\frac{MW_{NO_x}}{MW_{mix}}[NO_x]\right)k_{hg}\dot{m}_{exh}}{P_i} \quad (16)$$

$$ISTHC = \frac{\left(\Sigma\frac{MW_{C_iH_j}}{MW_{mix}}[C_iH_j] + \frac{MW_{ETOH}}{MW_{mix}}[ETOH] + \frac{MW_{MECHO}}{MW_{mix}}[MECHO]\right)\dot{m}_{exh}}{P_i} \quad (17)$$

Where MW_i is the molar ratio of specie i, MW_{mix} is the molar ratio from the mixture, $[i]$ is the molar fraction of specie i, $\dot{m}_{exh}$ is the total exhaust mass, k_{hg} is the correction applied to NO_x as a function of humidity and temperature and P_i is the indicated power.

2.2 Experimental setup description

The experiments were performed using an in line three cylinders DI turbocharged Ford EcoBoost 1.0 liters engine. The engine is equipped with four valves per cylinder and double overhead camshaft (DOHC), with a twin independent variable cam timing (Ti-VCT) system. Engine specifications are shown in Table 1.

Table 1: Engine specifications

Parameter	Description
Displaced Volume	999 cc
Number of Cylinders	3
Stroke	82 mm
Bore	71.9 mm
Connecting Rod	137 mm
Compression Ratio	10:1
Number of Valves per	4
Exhaust Valve Open	38° BBDC @ 0.5 mm
Exhaust Valve Close	10° ATDC @ 0.5 mm
Inlet Valve Open (IVO)	10° BTDC @ 0.4 mm
Inlet Valve Close (IVC)	38° ABDC @ 0.5 mm
Injection	High pressure direct injection with 6 holes
Combustion Chamber	Pent-roof

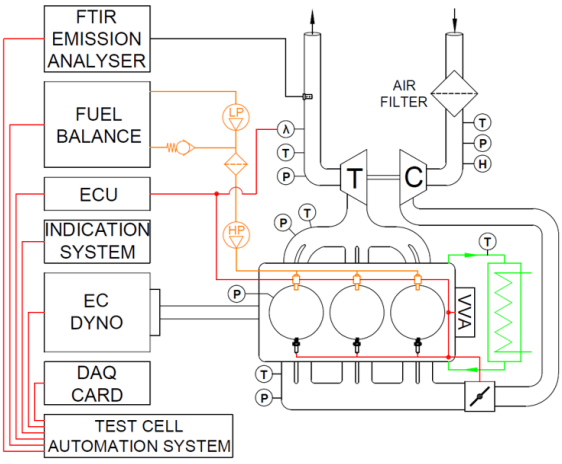

Figure 1: Experimental setup scheme

For the acquisition of intake and exhaust pressure a MPX4250 and an AVL APT100 pressure transducers were used, respectively. The intake temperature was measured using an AVL PT100 sensor. Temperatures of the exhaust gas, before and after the turbine, oil reservoir and cooling system were monitored with a K type thermocouple. Atmospheric air pressure, temperature and humidity were measured utilizing a HMT330 unit from VAISALA. A programmable engine control unit (ECU) Bosch MS6.3 was used to adjust engine operating parameters, such as angle of start of injection, angle of ignition, valve phase timing and others. The monitoring of air-fuel mixture was carried out using a Bosch LSU 4.9 lambda probe.

For the acquisition and processing of the in-cylinder pressure signal were used an AVL GH14D piezoelectric pressure transducer and the indicated system AVL IndiMicro 602. The online analysis of combustion parameters was performed by AVL Indicom user interface software. The engine load was applied through an AVL DynoPerform 240 dynamometer. Fuel consumption was obtained using an AVL 7130 fuel balance with principle based on gravimetric measurement. The combustion products were measured with the AVL Sesam FTIR i60 emission analyser. The AVL PUMA Open system was used to control the test cell and simultaneous data acquisition. The experimental setup scheme is shown in Figure 1.

2.3 Test procedure

The engine was warmed up for 20 minutes at medium load before each test condition. The engine oil and coolant temperatures were maintained at 365±2 K. The fuel used was hydrous ethanol E94W06 (6% v/v water content) and the air-fuel ratio was stoichiometric. The tests conditions were performed at 1500 rpm and the spark advance was adjusted to kept CA50 at 10 CAD ATDCf. The variable valve timing from intake and exhaust valves were fixed at -10 and 10 CAD ATDCi respectively, which represent a positive valve overlap (PVO) of 20 CAD at 0.5 mm of valve lift as shown in Figure 2.

The maximum brake load at 1500 rpm is 16 bar of brake mean effective pressure (BMEP) for this engine (López et al. 2020). Then, the maximum partial load considered for this work was 8 bar IMEP. Two different engine loads were tested: 2 and 8.0 bar IMEP. The engine variability was measured through COV of IMEP and the maximum allowed value was of 3.0% for stable combustion and as a limit for vehicle homologation and drivability (Heywood 2018).

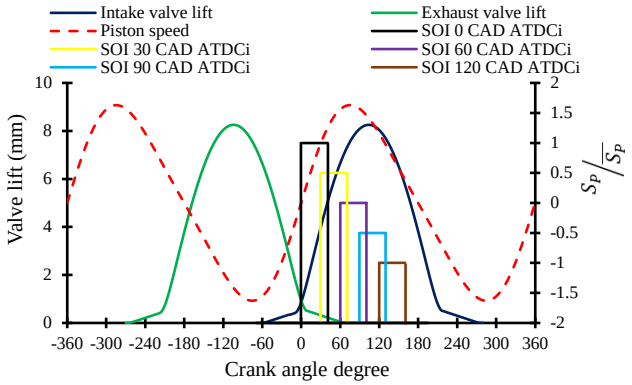

Figure 2: Valve lift, piston speed and SOI tested to 100 bar injection pressure as a function of crank angle degree

3. RESULTS

Figure 3 shows the intake pressure as a function of injection timing and pressure for two different engine loads. The intake pressure decreases as the injection timing is retarded. The main reason is due the cooling effect, which results in higher air specific gravity due the lower temperature. Therefore, the throttle opening is closed to decrease the intake pressure and thus maintain the same engine load. The relative decreasing on intake pressure were 8.6 % in 8 bar IMEP and 10 % in 2 bar IMEP considering the start of injection (SOI) in 0 and 120 CAD ATDCi. However, the cooling effect is more pronounced in higher load, despite the relative difference of pressure be almost the same in both loads. This effect is easily visualized by the absolute intake pressure difference value. As can be seen, the pressure reduction rate in 8 bar IMEP is higher than in 2 bar IMEP as the SOI is delayed. The reason is the large injected fuel mass that requires more heat to full vaporization. In addition, the fuel heat absorbed during injection event tends to come from air instead from in-cylinder surrounding as late as the SOI. In Figure 2 is shown the piston speed and the SOI for 100 bar injection pressure. The in-cylinder air flow is proportional to piston speed. Thus, late injection timing results in a more pronounced cooling effect.

Combustion parameters as CA10, CA50, CA90 and spark timing are depicted in Figure 4 as function of injection timing and pressure for 8 bar IMEP. The spark timing was retarded until SOI in 90 CAD and subsequently the spark timing was advanced to keep the CA50 in 10 CAD ATDCf. The main reason is the inhomogeneous mixture, resulting from the shorter time available for the proper formation of the stoichiometric mixture. Thus, the poor formation of the mixture leads to slightly rich regions around the spark plug. This can increase the reaction rate due the maximum in-cylinder temperature be achieved with slightly rich lambda. In this way, the spark timing need be retarded due the higher combustion velocity and then maintain constant combustion phasing. However, the cooling effect and poor formation of mixture is more pronounced for later injection timing. Thus, the spark timing was advanced to compensate the slow combustion caused by the lower in-cylinder temperature.

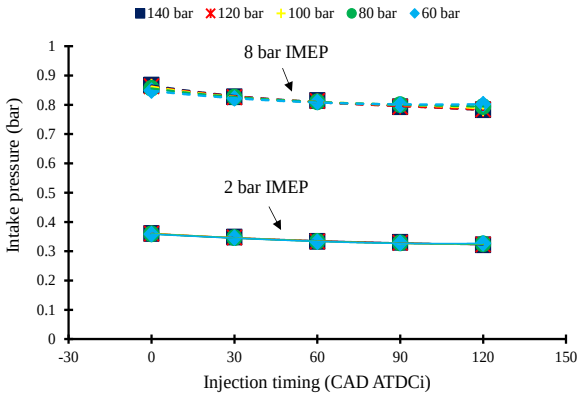

Figure 3: Intake pressure as a function of injection timing and pressure

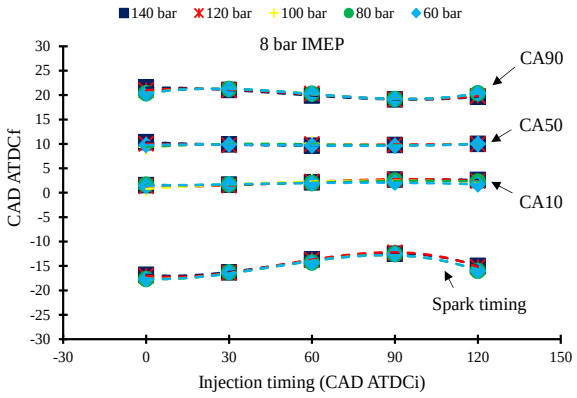

Figure 4: CA10, CA50, CA90 and spark timing for 8 bar IMEP as a function of injection timing and pressure

The maximum in-cylinder temperature for 2 and 8 bar IMEP are shown in Figure 5 as a function of injection timing and pressure. The maximum in-cylinder temperature (during combustion) was higher at late injection timing even with delayed spark timing. This is due, most probably, due to the reduced time for fuel vaporization and charge cooling with late injection, which, in turn, would lead to a decreased charge homogeneity.

The combustion duration is depicted in Figure 6 as a function of injection timing and pressure for 2 and 8 bar IMEP. Combustion duration decreased with delayed injection timing. The main reason could be the higher combustion velocity resulting from rich regions around spark plug. As discussed before, the increase in inhomogeneous mixture as retarded injection timing can increase the reaction rate as higher the rich region around the spark plug until the cooling effect and poor mixture formation play a greater role and then decrease the combustion velocity. Also, the injection pressure has an effect on combustion duration mainly for 2 bar IMEP and late injection in 8 bar IMEP. The atomization of the fuel decreases as lower the injection pressure, decreasing the relation between surface area and volume from liquid fuel drops and then increase the time for fully vaporization. Thus, poor formation of the mixture is expected as lower the injection pressure, increasing the combustion duration. This effect was more pronounced in 2 bar IMEP, where the higher residual gas fraction could also impair the combustion duration. In addition, the effects of injection pressure are more distinct in later injection timings, due to short time for proper mix.

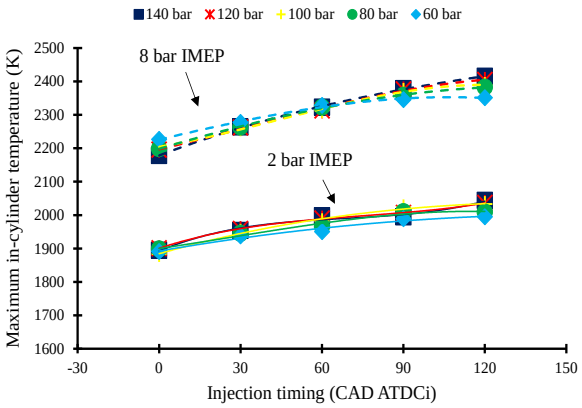

Figure 5: Maximum in-cylinder temperature as a function of injection timing and pressure

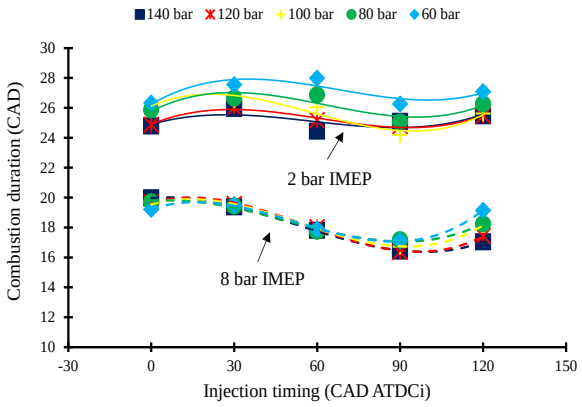

Figure 6: Combustion duration as a function of injection timing and pressure

In Figure 7 is shown the effects of injection timing and pressure in combustion variability. For 8 bar IMEP the COV_{IMEP} was less sensitive due lower residual gas fraction and higher in-cylinder pressure and temperature. Therefore, remained almost constant in all injection timings and pressures. However, at 2 bar IMEP the effects of injection timing and pressure were more pronounced. The higher residual gas fraction than 8 bar IMEP caused higher combustion variability. Fuel impingement could happen in SOI at 0 CAD due the fuel injection occurs near the piston. In late injection timing, the less time to proper mixture formation can increase the combustion variability. However, the higher injection pressure reduces the COV_{IMEP} due the better fuel atomization, which improves the mixture formation. The COV_{IMEP} remained below 3% in all tested condition. Nevertheless, for low loads the maximum acceptable value is 2% of COV_{IMEP}

for smooth engine operation (Heywood 2018). The only tested condition with acceptable COV_{IMEP} for 2 bar IMEP was the SOI at 30 CAD ATDCi.

The indicated specific carbon monoxide (ISCO) emission is shown in Figure 8 as a function of injection timing and pressure. For SOI at 0 CAD ATDCi, the fuel impingement could has caused incomplete combustion, resulting in higher CO emissions for both engine loads. Furthermore, CO emission was higher as delayed injection timing, due less time available for complete mixture mainly for 2 bar IMEP. This effect was less pronounced in 8 bar IMEP than 2 bar IMEP due higher in-cylinder pressure and temperature, which increase the combustion velocity. In addition, CO decreased as greater the injection pressure due better fuel atomization, resulting in a better homogenized mixture.

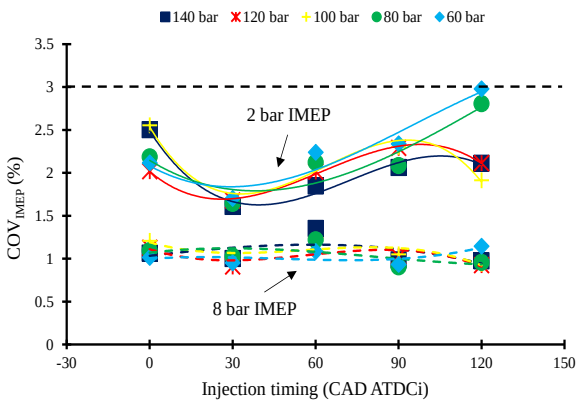

Figure 7: COV_{IMEP} as a function of injection timing and pressure

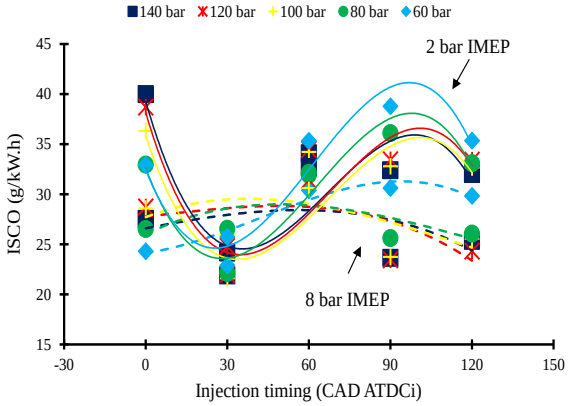

Figure 8: Indicated specific carbon monoxide emission as a function of injection timing and pressure

Figure 9 depicts the indicated specific total hydrocarbons (ISTHC) emissions as a function of injection timing and pressure for 2 and 8 bar IMEP. There were high levels of hydrocarbons emissions in 8 bar IMEP for SOI at 0 CAD ATDCi. The possible explanation is the fuel impingement on the top of the piston. SOI of 30 CAD ATDCi showed lower ISTHC for both loads. Delayed injection timings increased hydrocarbons emission due inhomogeneous mixture. For both loads, lower injection pressure showed an increase in THC emissions, as a result of poor fuel atomization.

The indicated specific nitrogen oxides ($ISNO_X$) is shown in Figure 10 as a function of injection timing and pressure. The NO_X emission was lower for 2 bar IMEP than 8 bar IMEP. The main reason is the lower in-cylinder temperature, which reduces NO_X formation rate. For 8 bar IMEP, the levels of NOx increased with later injection timings due higher in-cylinder temperature as seen in Figure 5, which can be resulted from rich region around spark plug. The amount of fuel injected provides stoichiometric air-fuel ratio. Thus, considering that the inhomogeneous mixture could leads rich region around the spark plug, the burned gas would end with an oxygen availability. This would enhancer the NO_X formation in high temperature. The poor formation of the mixture due lower injection pressure can intensify the pollutant formation as the inhomogeneous mixture increase.

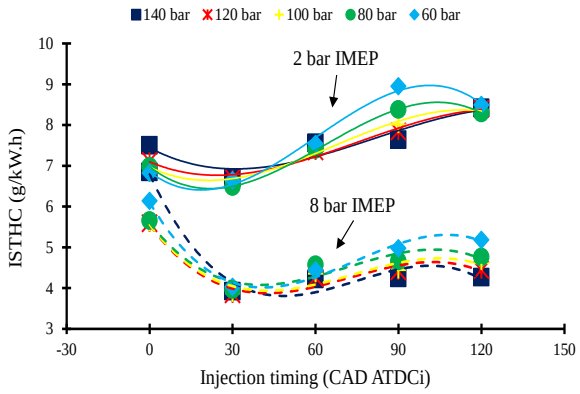

Figure 9: Indicated specific total hydrocarbons emission as a function of injection timing and pressure

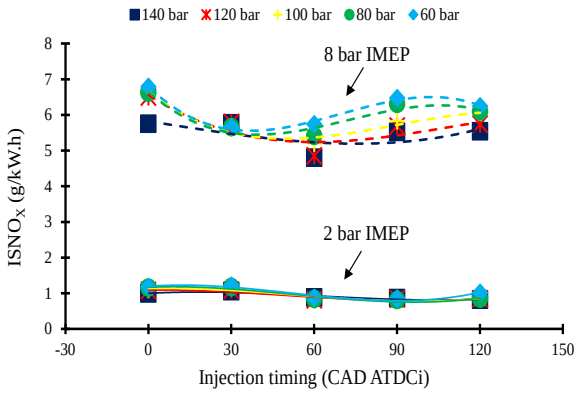

Figure 10: Indicated specific nitrogen oxides emission as a function of injection timing and pressure

Figure 11 shows the combustion efficiency resulted as a function of injection timing and pressure for 2 and 8 bar IMEP. The best combustion efficiency was reached with the SOI set in 30 CAD ATDCi for both engine load, despite the lower value difference among the tested conditions.

The indicated efficiency is depicted in Figure 12 as a function of injection timing and pressure. The indicated efficiency remained basically constant for all injection timing and pressure tested. The injection timings and pressure had a greater effect in emissions and combustion stability than in fuel consumption.

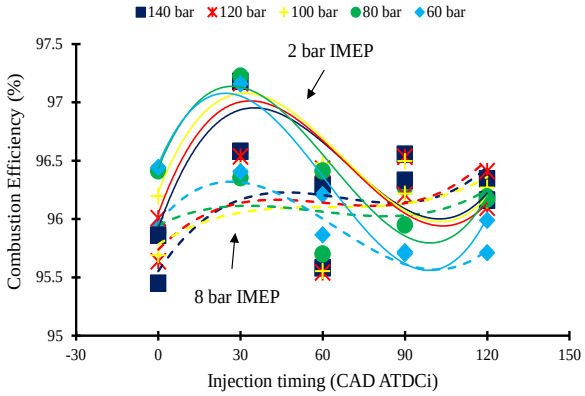

Figure 11: Combustion Efficiency as a function of injection timing and pressure

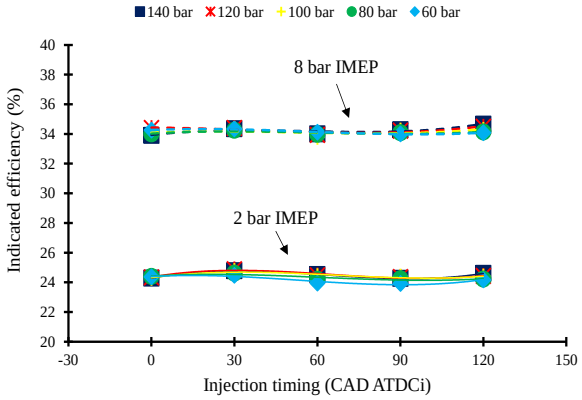

Figure 12: Indicated Efficiency as a function of injection timing and pressure

4. .CONCLUSIONS

The present study investigated the effects of injection timing and pressure on emissions and combustion performance parameters. The air-fuel ratio was set to stoichiometric condition and the experimental testes were carried out at 2 and 8 bar IMEP with CA50 fixed in 10 CAD ATDCf. The following conclusions could be drawn:

- SOI at 30 CAD ATDCi showed best results for combustion performance and emissions, due the better mixture homogenization.
- Fuel impingement at advanced SOI timing could be an important factor for combustion instability and higher levels of emissions.
- With lower injection pressures the fuel atomization potential was reduced, thus, increasing combustion duration and combustion variability.
- Cooling effect was more pronounced for late injection and high engine load due more in-cylinder air content and higher heat required to vaporization as increased fuel mass injected.
- Inhomogeneous mixture can result in rich region around spark plug, increasing combustion velocity and decreasing combustion duration.
- For 8 bar IMEP, the COV_{IMEP} were less sensitive due lower residual gas fraction and higher in-cylinder pressure and temperature than 2 bar IMEP.
- For 2 bar IMEP, the SOI at 30 CAD ATDCi was the only condition with COV_{IMEP} below 2%.
- CO and THC emissions increased for late injection timing due less time to proper mixture formation
- NO_X emissions increased for late injection due inhomogeneous mixture that resulted to higher in-cylinder temperature.

5. ACKNOWLEDGEMENTS

The authors would like to thank the Federal University of Santa Maria, Federal University of Rio Grande do Sul and the Coordination for the Improvement of Higher Education Personnel (CAPES) for the financial support of this project.

6. REFERENCES

Agência Nacional do Petróleo Gás Natural e Biocombustíveis - ANP. n.d. “RenovaBio.” Accessed May 17, 2020. http://www.anp.gov.br/producao-de-biocombustiveis/renovabio.

Bassett, Michael, Jonathan Hall, Tony Cains, Mark Underwood, Richard Wall, and Bryn GR Richards. 2017. “Dynamic Downsizing Gasoline Demonstrator.” *SAE International Journal of Engines* 10 (3): 2017-01–0646. https://doi.org/10.4271/2017-01-0646.

Bejan, Adrian. 2016. *Advanced Engineering Thermodynamics*. Wiley. https://doi.org/10.1002/9781119245964.

Chincholkar, S.P., and J.G. Suryawanshi. 2016. “Gasoline Direct Injection: An Efficient Technology.” *Energy Procedia* 90 (December 2015): 666–72. https://doi.org/10.1016/j.egypro.2016.11.235.

Economic Commission for Europe of the United Nations. 2013. “Regulation No 49 of the Economic Commission for Europe of the United Nations (UN/ECE).” *Official Journal of the European Union* 171: 1–390.

Economist, The. 2017. “The Death of the Internal Combustion Engine.” *Economist Intelligence Unit N.A. Incorporated* 413 (9050).

ExxonMobil. 2019. “2019 Outlook for Energy: A Perspective to 2040,” 58.

Fraser, Neil, Hugh Blaxill, Grant Lumsden, and Mike Bassett. 2009. “Challenges for Increased Efficiency through Gasoline Engine Downsizing.” In *SAE Technical Papers*, 2:991–1008. https://doi.org/10.4271/2009-01-1053.

Germane, Geoff J, Carl G Wood, and Clay C Hess. 1983. “Lean Combustion in Spark-Ignited Internal Combustion Engines - A Review.” In *SAE Technical Papers*. https://doi.org/10.4271/831694.

Golke, D., J.L.S. Fagundez, N.P.G. Salau, and M.E.S. Martins. 2016. “Combustion Performance of N-Butanol, Hydrous Ethanol and Their Blends as Potential Surrogates for the Brazilian Gasoline.” *SAE Technical Papers* Part F1270 (October). https://doi.org/10.4271/2016-36-0274.

Golke, Diego, Thompson D.M. Lanzanova, Nina P.G. Salau, and Mario E.S. Martins. 2018. “Performance of Hydrous Ethanol, Butanol, and Their Blends in Comparison to Primary Reference Fuels on a Spark-Ignited Engine.” In *SAE Technical Papers*. https://doi.org/10.4271/2018-36-0194.

Hancock, Dave, Neil Fraser, Mike Jeremy, Richard Sykes, and Hugh Blaxill. 2008. “A New 3 Cylinder 1.2l Advanced Downsizing Technology Demonstrator Engine.” In *SAE Technical Papers*, 2008:776–90. https://doi.org/10.4271/2008-01-0611.

Hannah Ritchie and Max Roser. 2020. “CO_2 and Greenhouse Gas Emissions.” Our World in Data. 2020. https://ourworldindata.org/co2-and-other-greenhouse-gas-emissions.

Heywood, John B. 2018. *Internal Combustion Engine Fundamentals*. Edited by McGraw-Hill Education. 2º.

Kalghatgi, Gautam. 2018. “Is It Really the End of Internal Combustion Engines and Petroleum in Transport?” *Applied Energy* 225 (May): 965–74. https://doi.org/10.1016/j.apenergy.2018.05.076.

———. 2019. “Development of Fuel/Engine Systems—The Way Forward to Sustainable Transport.” *Engineering* 5 (3): 510–18. https://doi.org/10.1016/j.eng.2019.01.009.

Lanzanova, Thompson, Macklini Dalla Nora, André Aronis, Mario Martins, and Vitor Cogo. 2017. “Effects of Injection Timing on Performance, Combustion and Emissions of a Gasoline DI Engine.” In *Procceedings of the 24th ABCM International Congress of Mechanical Engineering*. ABCM. https://doi.org/10.26678/ABCM.COBEM2017.COB17-1496.

Lanzanova, Thompson Diórdinis Metzka, Macklini Dalla Nora, and Hua Zhao. 2016. “Performance and Economic Analysis of a Direct Injection Spark Ignition Engine Fueled with Wet Ethanol.” *Applied Energy* 169: 230–39. https://doi.org/10.1016/j.apenergy.2016.02.016.

Leone, Thomas G., James E. Anderson, Richard S. Davis, Asim Iqbal, Ronald A. Reese, Michael H. Shelby, and William M. Studzinski. 2015. “The Effect of Compression Ratio, Fuel Octane Rating, and Ethanol Content on Spark-Ignition Engine Efficiency.” *Environmental Science and Technology* 49 (18): 10778–89. https://doi.org/10.1021/acs.est.5b01420.

López, J. Javier, Antonio García, Javier Monsalve-Serrano, Vitor Cogo, and Karsten Wittek. 2020. “Potential of a Two-Stage Variable Compression Ratio Downsized Spark Ignition Engine for Passenger Cars under Different Driving Conditions.” *Energy Conversion and Management* 203. https://doi.org/10.1016/j.enconman.2019.112251.

MMA. 2018. “Resolução Conselho Nacional Do Meio Ambiente Nº 492” 1: 2002.

Nakata, Koichi, Shintaro Utsumi, Atsuharu Ota, Katsunori Kawatake, Takashi Kawai, and Takashi Tsunooka. 2006. “The Effect of Ethanol Fuel on a Spark Ignition Engine.” In . https://doi.org/10.4271/2006-01-3380.

Pielke, Roger. 2019. “Net-Zero Carbon Dioxide Emissions By 2050 Requires A New Nuclear Power Plant Every Day.” Forbes. 2019. https://www.forbes.com/sites/rogerpielke/2019/09/30/net-zero-carbon-dioxide-emissions-by-2050-requires-a-new-nuclear-power-plant-every-day/#7c8b7ef335f7.

Sari, R.L., D. Golke, H.J. Enzweiler, N.P.G. Salau, F.M. Pereira, and M.E.S. Martins. 2018. “Exploring Optimal Operating Conditions for Wet Ethanol Use in Spark Ignition Engines.” *Applied Thermal Engineering* 138 (June): 523–33. https://doi.org/10.1016/j.applthermaleng.2018.04.078.

Sari, R.L., D. Golke, H.J. Enzweiler, K.F. Santos, N.P.G. Salau, M.E.S. Martins, and F.M. Pereira. 2017. “Investigation of Compression Ratio Effect on Wet Ethanol Use in Spark Ignition Engines.” *SAE Technical Papers* 2017-Novem

(November). https://doi.org/10.4271/2017-36-0208.

Serrano, José. 2017. “Imagining the Future of the Internal Combustion Engine for Ground Transport in the Current Context.” *Applied Sciences* 7 (10): 1001. https://doi.org/10.3390/app7101001.

Stein, Robert A, Christopher J House, and Thomas G Leone. 2009. “Optimal Use of E85 in a Turbocharged Direct Injection Engine.” *SAE Technical Paper* 01 (1490): 670–82. https://doi.org/10.4271/2009-01-1490.

Thewes, Matthias, Martin Müther, Adrien Brassat, Stefan Pischinger, and Andreas Sehr. 2012. “Analysis of the Effect of Bio-Fuels on the Combustion in a Downsized DI SI Engine.” *SAE International Journal of Fuels and Lubricants* 5 (1): 274–88. https://doi.org/10.4271/2011-01-1991.

Yu, Xiumin, Zezhou Guo, Ping Sun, Sen Wang, Anshi Li, Hang Yang, Zhe Li, Ze Liu, Jingyuan Li, and Zhen Shang. 2019. “Investigation of Combustion and Emissions of an SI Engine with Ethanol Port Injection and Gasoline Direct Injection under Lean Burn Conditions.” *Energy* 189 (xxxx): 116231. https://doi.org/10.1016/j.energy.2019.116231.

Zhang, J., K. Nithyanandan, Y. Li, C.-F. Lee, and Z. Huang. 2015. “Comparative Study of High-Alcohol-Content Gasoline Blends in an SI Engine.” *SAE Technical Papers* 2015-April (April). https://doi.org/10.4271/2015-01-0891.

7. RESPONSIBILITY NOTICE

The authors are the only responsible for the printed material included in this paper.